# Electron–acoustic-phonon interaction and resonant Raman scattering in Ge quantum dots: Matrix and quantum confinement effects

Jean-Roch Huntzinger,* Adnen Mlayah, Vincent Paillard, Anja Wellner, and Nicolas Combe
*Laboratoire de Physique des Solides, UMR 5477 Université P. Sabatier–CNRS, 118 route de Narbonne, 31062 Toulouse Cedex 4, France*

Caroline Bonafos
*Centre d'Elaboration des Matériaux et d'Etudes Structurales, UPR 8011 CNRS, 29 Rue Jeanne Marvig BP 94347 Toulouse, France*
(Received 20 April 2006; revised manuscript received 27 July 2006; published 14 September 2006)

Calculations of the electron-acoustic phonon interaction, and Raman scattering efficiency, in matrix embedded Ge quantum dots (QDs) are presented. The work is focused on the understanding of the inelastic light scattering process excited close to resonance with the confined $E_1$ transitions. Due to the large joint density of states at the $E_1$ point, many intermediate electronic states contribute to the overall scattering efficiency. This particular situation leads to quantum interference effects between different scattering paths and has, therefore, a strong impact on the Raman line shapes and intensities. Quantum confinement of the electron and hole states is treated within the envelope wave function approximation. The QD/matrix acoustic vibrations are deduced from elasticity theory. Deformation-potential interaction between the electrons (and holes) and acoustic vibrations is assumed. The resonant Raman spectra are calculated using third order perturbation quantum theory. A Raman-Brillouin electronic density is constructed as a linear combination of the electronic states involved in the inelastic light scattering. It allows one to plot, for each excitation energy, the spatial distribution of the electronic density that gives rise to the Raman (or Brillouin) signal. It is calculated for both diagonal and off-diagonal transitions between the confined electronic states. The dependence of the spectral line shapes and intensities on homogeneous broadening of the $E_1$ transitions, QD size, surface boundary conditions is discussed in details. The calculated spectra are then compared to those measured for different QD size distributions.

DOI: 10.1103/PhysRevB.74.115308 PACS number(s): 78.67.Hc, 63.22.+m, 73.22.Lp, 78.30.Er

## I. INTRODUCTION

In some semiconductor quantum dot (QD) systems, for instance, Ge/Si, GaAs/AlAs, and InAs/InP, the acoustic impedance mismatch between the dot and the surrounding medium is rather small. The acoustic vibration modes are bulklike phonons extending over distances much larger than the QD size and even than the average separation between quantum dots. Therefore, Raman scattering, in the frequency range of acoustic vibrations, shows interference effects due to the spatial localization and correlation of the excited electronic states.[1–10] In contrast, localized acoustic vibrations[11–13] is a characteristic feature of semiconductor (CdS,[14–16] Si,[17–19] Ge[20–22]) and noble metal particles (Ag,[23–28] Au[27,29]) embedded in glass and polymers. In these systems, the coherence length of the vibration modes can be assimilated to the quantum dot size, leading so to incoherent light scattering. Then the Raman spectra are determined by quantum confinement of electronic states and acoustic modes localization in a single average QD.

In most of the published works, Raman scattering by confined acoustic vibrations is interpreted using the well-known Lamb's model.[30,31] This model describes the free vibrations of a homogeneous and isotropic elastic sphere: the displacement fields are obtained from Navier's equation which is solved by introducing scalar and vector potentials involving spherical harmonics labeled $(l,m)$ and spherical Bessel functions of the first kind. Continuity of the displacement and stress fields at the particle surface is imposed.[30,31] The eigenmodes are labeled by $l$ and $m$ and by the integer $n \geqslant 1$ in increasing order of eigenfrequencies. They are classified into spheroidal (breathing and twisting motion) and torsional (only twisting) modes. Using group symmetry arguments, Duval[32] concluded that only spheroidal modes [breathing $(n,l=0)$ and quadrupolar $(n,l=2)$ modes] are Raman active in agreement with experiments.

Dubrovski *et al.*[33] and Tamura *et al.*[34] extended Lamb's model to the vibrations of an elastic particle embedded in a homogeneous and infinite elastic matrix. Transmission of the QD vibrations to the surrounding medium was introduced using the spherical Hankel's function of the first kind for the displacement field outside the matrix. Therefore, radiation of vibrational energy from the particle to the surrounding medium becomes possible and homogeneous broadening of the acoustic modes appears, leading to complex valued eigenfrequencies.[19,33–35] The so-called complex frequency model (CFM) provides a good description of the matrix influence on the QD vibrations in terms of frequency shift and damping of eigenmodes.[36] However, orthonormalized displacement fields could not be obtained from the CFM, because their complex amplitudes diverge with increasing particle size. Properly normalized displacement fields are needed not only for a complete understanding of the matrix influence but also for the modeling of the electron-phonon interaction and Raman scattering efficiency.

Extending the work of Montagna and Dusi,[36] Murray and Saviot[19,37] have recently proposed a model which allows one to obtain orthonormalized displacement fields. In their core shell model (CSM) the spherical particle with radius $R_p$ occupies the center of a spherical cavity with radius $R_m \gg R_p$ representing the matrix.[38] The equation of motion is solved for $R_m$ and $R_p$, and the displacement vectors are orthonormal-

 

ized according to total energy conservation.[37]

Calculations of the Raman efficiency requires modeling of the vibration modes but also of the electronic states and electron-phonon interaction as well. First attempts to simulate the Raman spectra of embedded semiconductor quantum dots were reported by Montagna and Dusi.[36] These authors, however, assumed dipole-induced-dipole scattering which does not take into account the electronic structure explicitly and is therefore suitable for nonresonant Raman scattering, only. Nevertheless, the interplay between homogeneous and inhomogeneous broadening of the Raman lines was clarified in this work.

Sirenko *et al.*[39] and Gupalov and Merkulov[40] reported on acoustic phonons assisted spin-flip Raman scattering in CdS QD embedded in silica glass. They assumed deformation-potential electron-acoustic phonon interaction and used a quantum description of the light scattering process based on the envelope wave function approximation of the confined electronic states. Their work mainly concentrated on the influence of the complex valence band structure of CdS on the Raman selection rules and spectral line shapes. Moreover, in the work by Gupalov and Merkulov[40] the Raman spectral line shape was studied in details for nonresonant scattering only. Whereas, Sirenko *et al.*[39] considered bulklike acoustic phonons for the calculation of the resonant Raman spectra; quantum confinement of acoustic vibrations was disregarded because the sound velocities and densities of CdS and silica glass differ only a little. Hence, the dependence of the resonant Raman line shapes and intensities, associated with localized acoustic phonons, on the particle size, excitation energy, and boundary conditions is still an open question.

In this work we present calculations of the electron-acoustic phonon interaction and Raman-Brillouin scattering efficiency following the approach developed by Sirenko *et al.*[39] and Gupalov and Merkulov.[40] It is adapted to the special case of Ge quantum dots embedded in $SiO_2$ and excited close to resonance with the $E_1$ gap. Size-quantization of both electron and hole states is treated within the envelope wave function approximation as in Refs. 39 and 40. The acoustic vibration modes are calculated following the method introduced by Montagna and Dusi.[36] We have investigated the two extreme situations where the particle surface moves freely or is rigidly fixed, as well as the intermediate situations. Deformation potential interaction between the confined electronic states and the acoustic vibrations is assumed. Due to the high joint density of states at the $E_1$ point, many electronic states are optically excited and contribute to the light scattering process. We have calculated the electron-phonon matrix elements for both diagonal and off-diagonal transitions between the confined electronic states and studied how their relative weight changes with the particle size. A Raman-Brillouin electronic density is introduced. It is constructed as a linear combination of the confined electronic states that are involved in the light scattering process. It allows us to determine, for each excitation energy, the spatial distribution of the effective electronic density that contributes to the Raman signal. We have studied the influence of the QD size, surface boundary conditions, and excitation energy (resonance effects). The calculated Raman spectra are compared to those measured for various Ge quantum dot sizes.

## II. THEORY

### A. Resonant Raman scattering

Our starting point is the usual third order perturbation theory of resonant Raman scattering.[41] The scattering amplitude for transition from state $|i\rangle$ to state $|f\rangle$ is dominated by the term

$$A_{i,f} = \sum_{a,b} R_\beta^{\mathrm{em}} R_\alpha^{\mathrm{abs}} \langle b|H_{\mathrm{e\text{-}v}}|a\rangle. \tag{1}$$

The sum is carried over all possible intermediate states $|a\rangle$ and $|b\rangle$. The states denoted by roman letters are composed of the photons and phonons baths and the electronic states. The latter are denoted by $|\alpha\rangle$ and $|\beta\rangle$ in $|a\rangle$ and $|b\rangle$, respectively. All the information on the resonance (denominator) and the optical oscillator strength (numerator) is carried by the two terms:

$$R_\beta^{\mathrm{em}} = \frac{\langle f|H_{\mathrm{e\text{-}r}}|\beta\rangle}{(E_\beta + \hbar\omega - \epsilon_i) - i\Gamma_\beta}, \tag{2a}$$

$$R_\alpha^{\mathrm{abs}} = \frac{\langle \alpha|H_{\mathrm{e\text{-}r}}|i\rangle}{(E_\alpha - \epsilon_i) - i\Gamma_\alpha}, \tag{2b}$$

where $E_{\alpha(\beta)}$ and $\Gamma_{\alpha(\beta)}$ are the energy and homogeneous broadening of the $\alpha$ and $\beta$ states, respectively. $\hbar\omega = \epsilon_i - \epsilon_f$ is the difference between incident and scattered photon energies. Generally, the electron-phonon interaction Hamiltonian may be written as

$$H_{\mathrm{e\text{-}v}} = \sum_\nu \underline{H}_{\mathrm{e\text{-}v}}(\nu) b_\nu + \mathrm{H.c.}, \tag{3}$$

where $\underline{H}_{e\text{-}v}(\nu)$ acts only on the electronic states. $b_\nu$ and its hermitic conjugate are the usual annihilation and creation operators of the phonon mode $\nu$.

Then the Raman intensity is proportional to

$$I(\omega) \propto \sum_{\nu/\omega_\nu = |\omega|} |A_\nu|^2, \tag{4}$$

where $A_\nu$ is the scattering amplitude from state $|i\rangle$ with an incident photon $\vec{k}_i$ to state $|f\rangle$ with a scattered photon $\vec{k}_f$, through emission or absorption of a phonon mode $\nu$ with energy $\hbar\omega_\nu$. The restriction $\omega_\nu = |\omega|$ ensures the overall energy conservation rule. For a phonon emission (Stokes process, $\omega > 0$):

$$A_\nu = \sqrt{N_\nu + 1}\,\underline{A}_\nu, \quad \text{with} \tag{5a}$$

$$\underline{A}_\nu = \sum_{\alpha,\beta} R_\beta^{\mathrm{em}} R_\alpha^{\mathrm{abs}} \langle \beta|\underline{H}_{\mathrm{e\text{-}v}}(\nu)|\alpha\rangle. \tag{5b}$$

For a phonon absorption (Anti-Stokes process, $\omega < 0$), the expressions are similar, only changing to $\sqrt{N_\nu}$ and $\underline{H}_{\mathrm{e\text{-}v}}(\nu)^\star$. The average occupation number $N_\nu$ for the mode $\nu$ of the phonon bath at temperature $T$ is the Bose-Einstein factor $\langle N_\nu\rangle = n(\omega_\nu) = 1/\exp(\hbar\omega_\nu/k_B T) - 1$. Using the relation $n(\omega_\nu) + 1 = |n(-\omega_\nu)|$, the Raman efficiency for both Stokes and anti-Stokes scattering reads

$$I(\omega) \propto |n(-\omega)| \sum_{\nu/\omega_\nu=|\omega|} |\underline{A}_\nu|^2. \quad (6)$$

### B. Electron-phonon interaction

In a Raman scattering process the intermediate electronic excitation can be either free or bonded electron-hole pairs. Hence, both electron and hole states contribute to the electron-phonon interaction Hamiltonian

$$\underline{H}_{\text{e-v}}(\nu) = \underline{H}^e_{\text{e-v}}(\nu) + \underline{H}^h_{\text{e-v}}(\nu). \quad (7)$$

As a first approximation, we consider only the deformation-potential term due to the local dilation accompanying the phonon displacement:[42]

$$\underline{H}^{e(h)}_{\text{e-v}}(\nu) = D_{e(h)}(\vec{\nabla} \cdot \vec{\underline{u}}_\nu), \quad (8)$$

where $D_{e(h)}$ is the conduction (respectively, valence) hydrostatic deformation-potential energy at the $E_1$ point; $\vec{\underline{u}}_\nu$ is the phonon displacement:

$$\vec{\underline{u}}_\nu = \sqrt{\frac{\hbar}{2\omega_\nu}} \vec{u}_\nu(\vec{r}). \quad (9)$$

The square root term follows from the second quantification procedure, $\varrho(\vec{r})$ is the volumic mass of the material at point $\vec{r}$ and $\vec{u}_\nu(\vec{r})$ are the "wave functions" of the phonon mode $\nu$, orthonormalized in the sense of

$$\int d^3r\, \varrho(\vec{r}) \vec{u}_\nu(\vec{r})^* \cdot \vec{u}_{\nu'}(\vec{r}) = \delta_{\nu\nu'}. \quad (10)$$

This is imposed by the commutation rule $[b_\nu, b^\dagger_\nu] = \delta_{\nu\nu'}$. Then the vibration energy quantum is indeed $\hbar\omega_\nu$ and the intuitive result is again met that the energy of a vibration depends on its amplitude.

### C. Raman-Brillouin electronic density

#### 1. Definition

In the following, we assume free electron-hole pairs. The calculation, however, could be extended to include excitonic effects. Then the scattering amplitude is simply the sum of the electron and hole contributions $\underline{A}_\nu = \underline{A}^{\text{e}}_\nu + \underline{A}^{\text{h}}_\nu$ with, in $\{\vec{r}\}$ representation,

$$\underline{A}^{\text{e(h)}}_\nu = \mathcal{R} \int d^3r\, \rho^{\text{e(h)}}(\vec{r}) [\underline{H}^{\text{e(h)}}_{\text{e-v}}(\nu)](\vec{r}), \quad (11)$$

where

$$\mathcal{R} = \sum_\gamma R^{\text{em}}_\gamma R^{\text{abs}}_\gamma \quad (12)$$

is a resonance factor and $\rho^{e(h)}(\vec{r})$ the Raman-Brillouin electronic density (RBED) defined as

$$\rho^{e(h)}(\vec{r}) = \frac{1}{\mathcal{R}} \sum_{\{(\beta,\alpha)/\beta^{h(e)}=\alpha^{h(e)}\}} R^{\text{em}}_\beta R^{\text{abs}}_\alpha \psi^{e(h)}_\beta(\vec{r})^\star \psi^{e(h)}_\alpha(\vec{r}) \quad (13)$$

where $\psi^{e(h)}_\alpha(\vec{r})$ are the envelope wave functions for the electron (hole) part of the state $|\alpha\rangle$, respectively.

The resonance factor (12) has been introduced in Eq. (13) in order to normalize the RBED: for a complete set of orthonormalized $\alpha$ and $\beta$ states, the RBED (13) verifies

$$\int d^3r\, \rho^{e(h)}(\vec{r}) = 1. \quad (14)$$

$\rho^{e(h)}(\vec{r})$ is simply a linear combination of joint local electronic densities $\psi^{e(h)}_\beta(\vec{r})^\star \psi^{e(h)}_\alpha(\vec{r})$ weighted by the optical resonance factors associated with the photon absorption and emission [(2b) and (2a), respectively].

Strictly speaking, the RBED does not contain new physics with respect to the usual description based on Eq. (1). It is obtained by a mere rewriting of the usual resonant Raman efficiency with the main benefit that all information on the light scattering process (optical oscillator strengths, incoming and outgoing resonances, electron-photon interaction selection rules) is entirely contained in a *single* physical quantity [$\rho^e(\vec{r})$ or $\rho^h(\vec{r})$].

The sum in Eq. (13) runs over all possible intermediate electronic states with the following restriction: the hole part of $\alpha$ and $\beta$ states must be identical if the interaction with the vibrations occurs through the electron parts ($\underline{A}^e_\nu$ term), and vice versa. This is imposed by the fact that upon absorption or emission of a vibration mode, through a Raman process, the excited system returns to its initial electronic state (which is generally a fundamental state).

Generally, all electronic states should enter the RBED. So the RBED is a fundamental quantity for third order interaction processes. Nevertheless, among all the electronic states some of them do not interact with a given vibration mode due to selection rules associated with the electron-vibration interaction mechanism: these states are thus not physically relevant for the considered interaction. Here we have chosen to restrict the summation in Eq. (13) to the electronic states that interact with the pure radial ($l=0$) vibrations. This restriction makes the interpretation of the Raman spectra much easier and allows us to focus on the radial shape of the RBED. If all the electronic states were taken into account, the calculated Raman spectra would be exactly the same.

Physically, the RBED is the electronic density distribution that emits or absorbs a given vibration mode through a Raman process. It is specific to each vibration mode because of the above-mentioned restrictions [i.e., the Raman selection rules in Eq. (13)].

The evolution of the shape of low-frequency Raman scattering with different parameters can often be obtained by simply looking at the real-space integral of $\rho^{e(h)}(\vec{r})$ with the electron-phonon Hamiltonian in Eq. (11), as will be illustrated later.

#### 2. Electronic states

We assume a spherical quantum well, with an infinite confinement potential at the dot surface, owing to the large conduction and valence band offsets between Ge and $SiO_2$. Then, the electron or hole envelope wave functions read[43]

$$\psi_{n,l,m}(\vec{r}) = \frac{1}{j_{l+1}(\eta_{n,l})} \sqrt{\frac{2}{a^3}} j_l\left(\eta_{n,l} \frac{r}{a}\right) \bar{Y}^m_l(\theta,\phi), \quad (15)$$

where $a$ is the dot radius. The inclusion of $\eta_{n,l}$, i.e., the $n$th zero of the $j_l$ spherical Bessel function, ensures that the wave

functions vanish at the boundary $r=a$; $\bar{Y}_l^m(\theta,\phi)$ are the normalized spherical harmonic functions. The confinement energy associated with these states is

$$E^c_{n_e,l_e,n_h,l_h} = \frac{\hbar^2}{2a^2}\left(\frac{\eta^2_{n_e,l_e}}{m_e^*} + \frac{\eta^2_{n_h,l_h}}{m_h^*}\right) \tag{16}$$

$m_e^*$ and $m_h^*$ being the electron and hole effective masses, respectively. The model used here to describe the QD electronic structure is very simple. It is based on the parabolic band approximation and envelope wave function approximation applied to the confined $E_1$ electronic transitions of Ge. Actually, the energy-band structure of Ge is more complex, it is much better described throughout the Brillouin zone using the $\mathbf{k}\cdot\mathbf{p}$ theory as shown by Pollack and Cardona.[44,45] Moreover, the validity of the envelope wave function approximation becomes questionable for very small QDs (few nm) because on the one hand the concept of envelope wave function itself becomes meaningless; on the other hand the electronic states involving surface atoms become as important as those associated with the inner atoms. For instance, tight binding calculations of the QDs electronic structure would have been much more appropriate. Our aim in this work is to focus on the modeling of the Raman scattering in QDs. The calculations presented here can be greatly improved using a more realistic description of the QDs electronic structure.

#### *3. Resonance*

In the following we assume, as a first approximation, that both oscillator strength and homogeneous broadening of the optical transitions are independent of the electron-hole pair state. In this case the Raman-Brillouin electronic density is driven by the reduced homogeneous broadening

$$\Gamma' = \Gamma/E^c_{\text{fund}} \tag{17}$$

and the relative detuning

$$\delta' = [\epsilon_i - (E_1 + E^c_{\text{fund}})]/E^c_{\text{fund}} \tag{18}$$

between incident photon energy and the fundamental transition energy $E_1+E^c_{\text{fund}}$, where the lowest confinement energy is

$$E^c_{\text{fund}} = E^c_{1,0,1,0} = \frac{\hbar^2\pi^2}{2a^2}\left(\frac{1}{m_e^*} + \frac{1}{m_h^*}\right). \tag{19}$$

For quantum dots in the strong quantum confinement regime, the electronic density of states is discretized (i.e., $\Gamma' \ll 1$). As illustrated in Fig. 1 the resonance factor (12) shows well-separated Lorentzian peaks, of width $\Gamma'$, each time the excitation energy equals that of a confined electron-hole transition. This situation is achieved in most of the semiconductors for electronic states associated with zone-center band gap $E_0$.

For $\Gamma' \gg 1$, quantum effects due to the discrete nature of the electronic density of states are washed out by the strong homogeneous broadening of the confined levels. As mentioned above, this situation (that of Ge $E_1$ states) is most likely to occur with electronic states having large effective masses. The resonance profile (12), shown in Fig. 1, is a broadband centered around zero detuning (very weak blueshift). Starting from the low-energy wing (negative detuning), all excited states contribute to the scattering efficiency with the same phase with respect to that of the laser line. The interferences, between the scattering paths involving different intermediate states, are constructive. In addition to the resonance effect, the constructive interference effect leads to enhancement of the scattering efficiency for $\delta' \lesssim 0$. The high-energy wing originates from destructive interferences between the scattering paths associated with intermediate states above and below the excitation energy. Roughly speaking, for excitation well above the band gap ($\delta' \gg 1$), there are as many states above as below the excitation energy, leading to a complete vanishing of the scattering efficiency. As the excitation comes closer to the band gap ($\delta' \gtrsim 0$), there are fewer states below, and hence less destructive interferences.

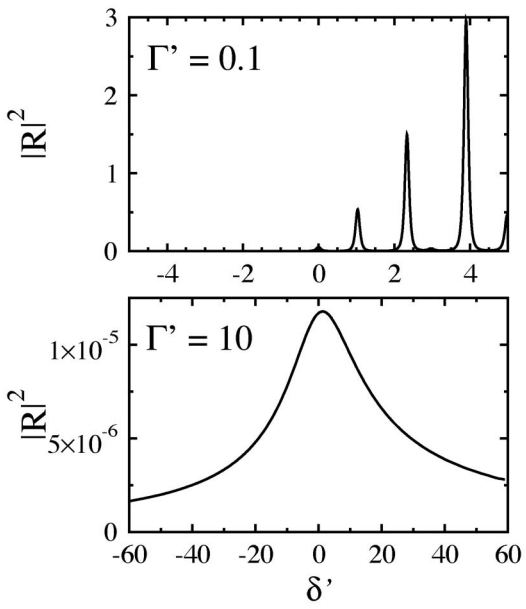


FIG. 1. Resonance profiles of the Raman scattering for reduced homogeneous broadening $\Gamma'=0.1$ and $\Gamma'=10$.

#### *4. On/Off-diagonal Raman Brillouin electronic density*

In low-dimensional systems, the electronic states are localized in real space at least in one direction. As already shown in several works on quantum wells[1,2,46,47] and QD multilayers,[3,7,39] this leads to the breakdown of the wave vector conservation in the Raman scattering process and hence to the activation of the phonon density of states.[48] It is worthwhile to underline that an important consequence of the electron wave function localization is that diagonal matrix elements for the electron-phonon interaction become allowed. This is the main difference with bulk crystals for which only off-diagonal matrix elements are allowed. Takagahara[49] and Zimmermann[50] introduced a pure and a real dephasing channel[51,52] associated, respectively, with diagonal and off-diagonal (final state interaction) electron-phonon matrix elements. In the pure dephasing, only the phase of the wave function changes (while the probability

density remains unchanged). The real dephasing is associated with scattering to other states and hence both wave function mixing and phase fluctuations take place. Acoustic phonon sidebands observed at low temperature around the photoluminescence line of single QDs, confirmed that pure dephasing is the channel through which the acoustic vibrations are emitted (and absorbed) by a QD state. Moreover, Zimmermann and Runge[51] and Belitsky *et al.*[53] pointed out the importance of pure dephasing for resonant Rayleigh scattering.[54]

Here, we study the contributions of pure and real dephasing channels to the resonant Raman scattering by decomposing the Raman-Brillouin electronic density (13) as $\rho=\rho_{\mathrm{on}}+\rho_{\mathrm{off}}$; where the on-diagonal density $\rho_{\mathrm{on}}$ corresponds to $\alpha=\beta$ terms in the sum (13) and $\rho_{\mathrm{off}}$ to $\alpha\neq\beta$ terms.

Let us consider, first, the case of a nanosized quantum dot with radius much smaller than the incident (and scattered) photon wavelength ($\lambda\sim 500$ nm): $ka\ll 1$ (with $k=2\pi/\lambda$). Then, the vector potential field $\vec{A}_k(\vec{r})$ inside the QD is quasiuniform and the reduced Hamiltonian $H_{\mathrm{e\text{-}r}}$ in (2a) and (2b) that acts on the envelope electronic functions is constant.[55] This imposes that the electron and hole wave functions of the pair created at the photon absorption step are identical: $\alpha_e=\alpha_h$. In the same way we have at the photon emission step $\beta_e=\beta_h$. In addition, for a Raman process mediated by the electron states, the hole state remains unchanged: $\beta_h=\alpha_h$ (geminate recombinations). Then only diagonal electron-phonon matrix elements are allowed: $\beta_e=\alpha_e$. It appears that, independently from the electron-phonon interaction mechanism, only pure dephasing processes do contribute to the Raman scattering in quantum dots.

Figure 2 shows the radial distribution of the RBED inside a QD with $a=4.5$ nm$\ll\lambda$. It is constructed only with diagonal matrix elements, and both electron and hole contributions were taken into account. The excitation energy is resonant with the fundamental electron-hole transition. The latter is, therefore, efficiently selected by the optical probe when $\Gamma'=0.1$. Then the RBED $\rho_{\mathrm{on}}(\vec{r})$ reduces to the electronic density associated with the first electron and hole states.

$$\rho_{\mathrm{on}}(\vec{r})=|\psi_{1,0,0}(\vec{r})|^2=\frac{\pi}{2a^3}\left(\frac{\sin\left(\pi\frac{r}{a}\right)}{\pi\frac{r}{a}}\right)^2. \qquad (20)$$

When $\Gamma'=10$, many (diagonal) electron-hole transitions come into resonance. As a consequence, the RBED is quasiuniformly distributed inside the QD (it is uniform in the quasiclassical limit $\rho_{on}=3/4\pi a^3$); around 1500 electron-hole transitions were used to generate the density distribution in Fig. 1. The vibration modes which may interact with the RBED shown in Fig. 1 are those responsible for a symmetric deformation field [see Eq. (8)], i.e., leading to nonvanishing values of the integral (11). This is the case of the $l=0$ and $l=2$ spheroidal modes.

We now consider a particle size comparable to the optical wavelength $ka\sim 1$. In that case, owing to the spatial variation of the vector potential field $\vec{A}_k(\vec{r})$, off-diagonal optical transitions between electron and hole states are allowed at both absorption and emission steps: $\beta_h=\alpha_h\neq\alpha_e\neq\beta_e$. Of course, this also means that off-diagonal electron-phonon

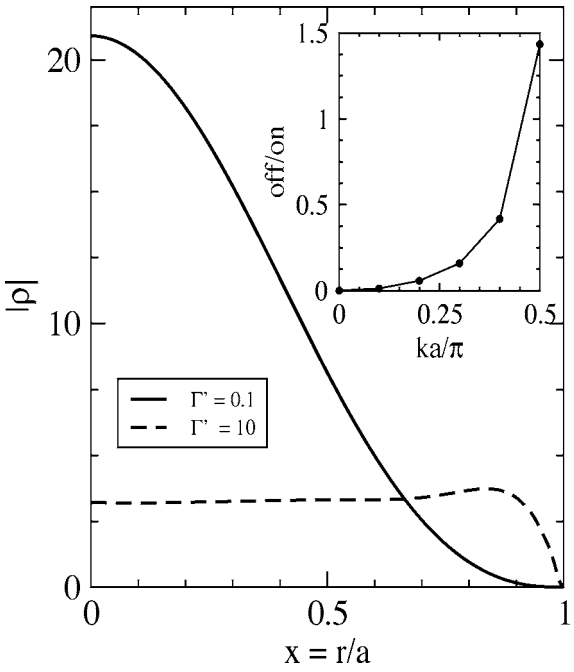


FIG. 2. Radial density distributions of the RBED in a QD with a=4.5 nm and for $\Gamma'=0.1$ and $\Gamma'=10$. The excitation is resonant with the fundamental confined electron-hole transition. The inset shows the change of the off/on RBED ratio $\int_0^1 dx\, x^2|\rho_{\mathrm{off}}(x)|/\int_0^1 dx\, x^2|\rho_{\mathrm{on}}(x)|$ as a function of $ka$, i.e., the ratio between particle size and photon wavelength.

matrix elements are allowed. The off-diagonal RBED $\rho_{\mathrm{off}}$ was calculated by decomposing the vector potential of the incident and scattered photons on a spherical basis. In order to keep within reasonable calculation times only the $l=0,1,2$ terms were retained. The inset of Fig. 2 shows the change of the ratio $\rho_{\mathrm{off}}/\rho_{\mathrm{on}}$ with particle size (or photon wavelength). For $ka\ll 1$, i.e., for nanosized QD, $\rho_{\mathrm{on}}\gg\rho_{\mathrm{off}}$ and only pure dephasing processes of the intermediate electronic states do contribute to the Raman scattering. While for $ka\gg 1$, $\rho_{\mathrm{on}}\ll\rho_{\mathrm{off}}$ which means that pure dephasing processes are washed out by the wave vector conservation law and hence only real dephasing is responsible for Raman scattering as expected for bulk semiconductors.

The infinite confinement approximation is not really a strong limitation of the model since the concept of RBED is quite general: It can be used for every set of electronic wave functions. Nevertheless, if one takes into account finite barrier height the electron and hole wave functions are no more exactly the same, because of the different electron and hole effective masses. Then, even for a particle size much smaller than the photon wavelength, the off-diagonal RBED could be nonzero. However, provided that the QD size is large compared to the penetration of the wave functions into the barrier (as in our case for several nanometer sized Ge QDs in $SiO_2$), this effect should not be important.

### D. Plane wave phonons

In order to point out only the effect of electronic wave function localization on the electron-phonon interaction and

Raman scattering, we first neglect the difference between the mechanical properties of the dot and the matrix (no acoustic mismatch). This approximation has been used by Sirenko *et al.*[39] for CdS QD embedded in $SiO_2$. Here, our aim is to study the characteristics of the Raman spectra in the case where a large number of localized intermediate electronic states contribute to the light scattering.

Bulklike acoustic phonons with wave vector $\vec{q}$ and polarization $\vec{e}_{\vec{q}}$ may be described by plane waves $\vec{u}_{\vec{q}}(\vec{r}) = \sqrt{1/\varrho V}\exp(i\vec{q}\cdot\vec{r})\vec{e}_{\vec{q}}$; their dispersion is linear over a wide range of the Brillouin zone: $\omega = c_l q$, $c_l$ being the sound velocity. Here, we consider only longitudinal vibrations, as transverse modes have a null divergence and therefore do not interact with electrons via the deformation-potential mechanism [Eq. (8)].

The interaction Hamiltonian (8) between electrons (or holes) and longitudinal acoustic phonons reads

$$\underline{H}^{e(h)}_{\text{e-v}}(\vec{q}) = D_{e(h)}\sqrt{\frac{\hbar}{2\varrho V\omega_{\vec{q}}}}iq\exp(i\vec{q}\cdot\vec{r}) \tag{21}$$

and using Eqs. (11) and (13) the Raman scattering intensity is given by

$$I^e(\omega,a) \propto |\mathcal{R}|^2 g(\omega)|n(-\omega)|\omega|M^e[q(\omega)a]|^2, \tag{22}$$

where, for a spherical quantum dot, the phonon density of states is three dimensional: $g(\omega)\propto\omega^2$. In principle, this calculation should involve the form factor

$$M^e_{\vec{q}} = \int d^3r\,\rho^e(\vec{r})\exp(i\vec{q}\cdot\vec{r}), \tag{23}$$

i.e., the Fourier transform of the Raman-Brillouin electronic density (13). But since in this paper we focus on isotropic displacements, we shall keep only the $l=0$ part of the plane wave in (21). Then the Raman efficiency is proportional to the square of

$$M^e[q(\omega)a] = \int dr\,r^2\rho^e(r)j_0(qr). \tag{24}$$

In principle, electron and hole contributions should be summed coherently. But in the infinite well and long wavelength approximation they are identical, leading so to the same Raman-Brillouin electronic density.

The Raman spectra calculated for a Ge quantum dot, with a radius $a=4.5$ nm, are shown in Fig. 3 for reduced homogeneous broadening $\Gamma'=0.1$, 1, and 10. In the inset of Fig. 3 are plotted the RBED distributions as a function of the distance $r$ to the center of the QD.

First, whatever the homogeneous broadening is, the RBED is localized in real space and therefore all acoustic-phonon modes contribute to the Raman scattering (see calculated spectra of Fig. 3); this is the well-known effect of a breakdown of the wave vector conservation law. Second, for weak reduced broadening ($\Gamma'=0.1$) only the fundamental confined electronic state is selected by the resonant optical excitation, and the low-frequency Raman spectrum is simply the Fourier transform of the corresponding density distribution [Eq. (20) and inset of Fig. 3] modulated by the frequency dependence of the electron-phonon interaction Hamiltonian, phonon density of states, and the Bose-Einstein population factor [see (22)]. For large homogeneous broadening ($\Gamma'=10$), the RBED is quasiuniformly distributed within the QD; its Fourier transform oscillates in the frequency domain (reciprocal space) leading to periodic intensity modulation of the Raman spectra. The main point we would like to underline in Fig. 3 is that even when a large number of electronic states do participate to the light scattering ($\Gamma'=1$ and 10), it is still possible to interpret and understand the Raman spectra in terms of electron wave function localization owing to a single effective electronic density, namely the RBED.

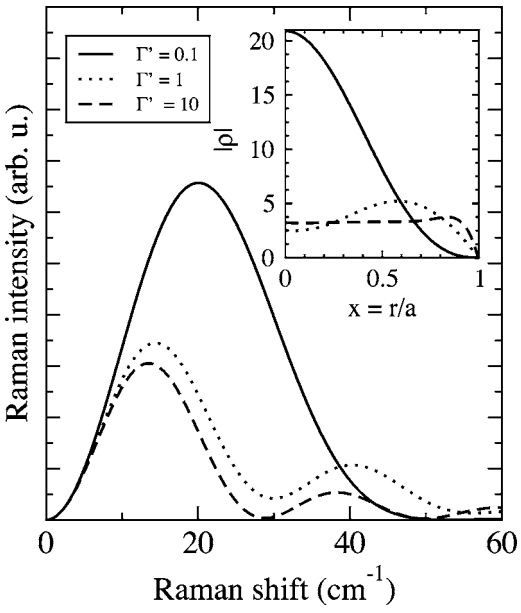


FIG. 3. Calculated Raman spectra of a Ge QD (radius $a=4.5$ nm) assuming plane wave acoustic phonons, and for $\Gamma'=0.1$, 1, and 10. The RBED used for the calculations of the Raman spectra are plotted in the inset for reduced homogeneous broadening $\Gamma'=0.1$ (solid line), 1 (dotted line), and 10 (dashed line). The optical excitation is resonant with the confined fundamental transition in all calculations.

### E. Acoustic mismatch

In the previous section, the difference between the mechanical properties of the dot and the surrounding medium was ignored. We now study the influence of the dot/matrix acoustic mismatch on the electron-phonon interaction and Raman spectra. As we recalled in the introduction, Gupalov and Merkulov[40] calculated the electron-phonon interaction and Raman spectra for the pure radial modes ($l=0$) of CdS QDs embedded in $SiO_2$. The vibration eigenvectors were obtained from the complex frequency model.[19,33–35] Here, we adopt the approach initially reported by Montagna and Dusi[36] and recently extended by Murray and Saviot.[19,37]

The starting point is the plane wave phonon modes discussed previously, but the vibration resonances that may

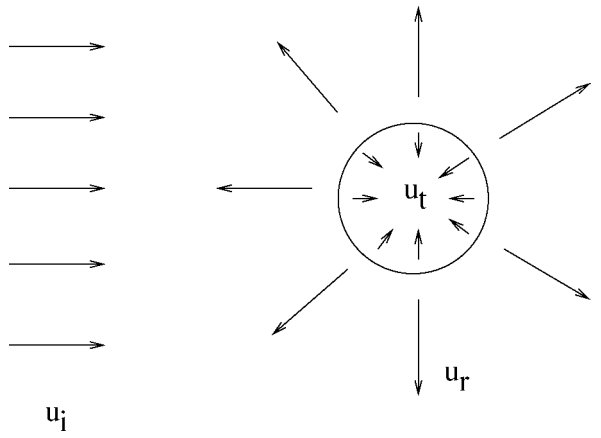


FIG. 4. Schematic representation of the incident $\vec{u}_i$, transmitted $\vec{u}_t$, and reflected $\vec{u}_r$ phonon displacements fields.

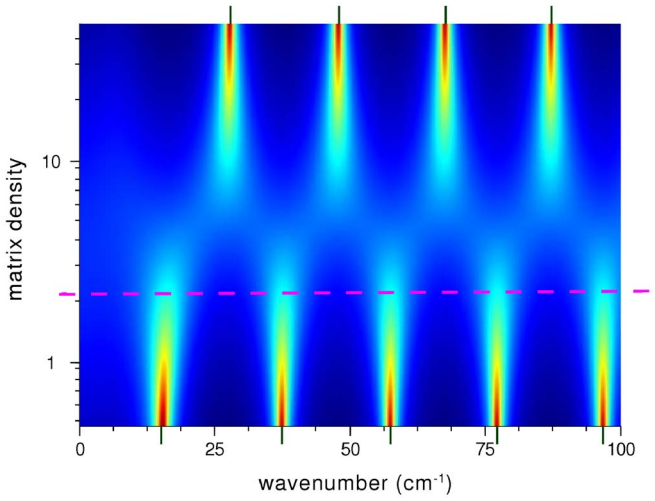


FIG. 5. (Color online) Modulus of the dilation coefficient $A^t_{0,0}$ plotted as $|A^t_{0,0}|/\omega$ versus incident phonon wave number $\omega$ and matrix density $\varrho_2$. The vertical ticks show the frequencies of the acoustic resonances in the situations where the QD surface moves freely or is rigidly fixed. The horizontal dashed line corresponds to $SiO_2$: $\varrho_2=2.21$.

occur inside the quantum dot are now taken into account: the vibration eigenmodes are determined as a superposition of an incident plane wave traveling inside the matrix, an elastically reflected (or scattered) wave and a transmitted wave into the quantum dot (see Fig. 4).

One important advantage of this method is, when the QD is much smaller than the matrix, and the acoustic mismatch not too high, one may assume that the vibration eigenmodes are automatically normalized, to a good approximation. Indeed the (matrix) phonons bath is not modified by the presence of the QD. Hence the amplitudes of the scattered and transmitted waves are determined by the mechanical boundary conditions to be fullfilled at the dot/matrix interface and by the amplitude of the incident plane-wave phonon mode [which is normalized according to Eq. (10)]. Moreover, because the mechanical boundary conditions are more easily expressed in spherical coordinates, we first decompose the incident plane wave as a sum of spherical modes $\vec{u}_{l,m}$ given in the Appendix

$$\vec{u}_i = u_0 \exp(i\vec{q}\cdot\vec{r})\vec{e}_{\vec{q}} = \sum_{l,m} \vec{u}_{l,m}, \tag{25}$$

where $u_0=1/\sqrt{\varrho V}$ is the incident phonon amplitude.

For longitudinal phonons ($\vec{\nabla}\times\vec{u}_i=\vec{0}$), the dilation field $\Lambda_i=\vec{\nabla}\cdot\vec{u}_i$ obeys Helmoltz's equation; according to Eq. (25), its decomposition on the $\vec{u}_{l,m}$ is given by

$$\Lambda^i_{l,m} = A^i_{l,m} z_l(qr) Y^m_l(\theta,\phi), \tag{26}$$

where, $z_l$ is the Bessel function of the first kind ($z_l \equiv j_l$), and $A^i_{l,m}$ the dilation coefficients.

$$A^i_{l,m} = u_0 q i^{l+1}(2l+1)\delta_{m,0}. \tag{27}$$

The coefficients $B^i_{l,m}$ and $D^i_{l,m}$ are found to be zero, consistent with the irrotational character of the longitudinal mode.

The vibration wave transmitted by the matrix to the QD is described by Bessel functions of the first kind $z_l \equiv j^{(1)}_l$ in order to ensure that the internal displacements remain finite. The vibrations reflected by the QD are outgoing waves described by the spherical Hankel function of the first kind $z_l \equiv h^{(1)}_l$. The coefficients $A^t_{l,m}, B^t_{l,m}, D^t_{l,m}, A^r_{l,m}, B^r_{l,m}, D^r_{l,m}$ are then obtained from the mechanical boundary conditions at the dot/matrix interface (see the Appendix).

Since the resonant electron-hole transitions excited in the Raman scattering are confined inside the QD, the electron-phonon interaction occurs within the QD. Moreover, according to Eq. (8) the electron-phonon interaction is proportional to the dilation field. Hence, the $A^t_{l,m}$ are the most important coefficients to look at.

Here, we focus on the pure radial modes ($l=0$) associated with the breathing motion of the QD. The modulus of the dilation coefficient $|A^t_{0,0}|$ is plotted in Fig. 5 for a Ge QD with radius $a=4.5$ nm. For a better scaling, $|A^t_{0,0}|$ has been divided by $\omega$, the frequency of the incident phonon mode. The upper and lower part of Fig. 5 are close to the situations of rigidly fixed and free surface, respectively.

First, one can notice that acoustic resonances occur at higher frequencies for a fixed QD surface than for a free surface, as is well known.[37] In both situations, the vibration density of states is discretized: confined vibration modes occur at particular frequencies determined by the QD size and by the sound velocities. In the intermediate situations, vibration modes appear at all frequencies and the acoustic resonances are homogeneously broadened due to the matrix/dot coupling. The contrast between the displacement fields inside the QD and in the matrix is minimum for $\varrho_2=4.82$. This value is close to the longitudinal impedance matching condition $\varrho_2=\varrho_1(c_{l,1}/c_{l,2})=4.74$. As already discussed by Saviot *et al.*,[29] the difference between these two values lies in the fact that the longitudinal impedance matching condition is valid for planar geometries (layered structures) and must be reconsidered in the case of a spherical geometry where both the longitudinal and transverse sound velocities are involved.

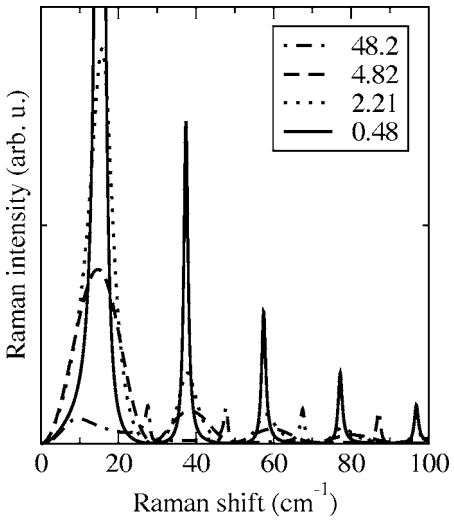


FIG. 6. Simulated resonant Raman spectra of a Ge QD embedded in $SiO_2$. The dot radius is $a=4.5$ nm and the RBED is quasiuniform $\Gamma'=10$. The QD/matrix acoustic mismatch is varied by changing the matrix density $\varrho_2$ from 0.48 to 48.2.

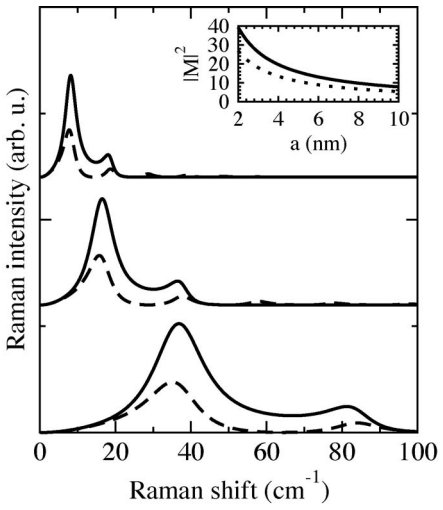


FIG. 7. Simulated Raman spectra for a Ge QD embedded in $SiO_2$. The dot radius is $a=9$, 4.5, and 2 nm from top to bottom. The continuous (respectively, dashed) lines are for $\Gamma'=0.1$ (respectively, $\Gamma'=10$). The corresponding form factors integrated up to 100 cm$^{-1}$ are shown in the inset.

Using Eqs. (22) and (25) the Raman scattering intensity is given by

$$I(\omega,a) \propto |\mathcal{R}|^2 g(\omega)|n(-\omega)|\frac{1}{\omega}|A^t_{0,0}|^2|M_{0,0}[q(\omega)a]|^2, \quad (28)$$

where $M_{0,0}[q(\omega)a]$ is the form factor [Eq. (24)] in which only the pure radial component of the plane wave expansion (25) has been retained.

The Raman spectra calculated, using Eq. (28), for different QD/matrix acoustic mismatch are shown in Fig. 6. The reduced homogeneous broadening is $\Gamma'=10$ and the detuning $\delta'=0$ (see Fig. 1). The excited RBED is quasiuniformly distributed inside the QD (Fig. 2). First, one can note that the linewidths of the Raman peaks associated with the acoustic resonances increase with increasing mechanical coupling between the dot and the matrix (i.e., homogeneous broadening of confined acoustic vibrations). This effect has been already discussed by Montagna and Dusi[36] for their spectra calculated using the dipole-induced-dipole scattering mechanism. As underlined by these authors, it has to be taken into account while evaluating the contributions of homogeneous and inhomogeneous broadenings to the total Raman linewidth. Second, from $\varrho_2=0.48$ (nearly free surface) to $\varrho_2=4.82$ (minimum contrast between the QD and the matrix displacement fields) the Raman peaks slightly shift towards lower frequencies. This is mainly due to the fact that both the Bose-Einstein factor and the form factor [Eq. (24)] enhance the contribution of the lowest frequency vibration modes. For a nearly fixed surface ($\varrho_2=48.2$) the acoustic resonances and Raman peaks are shifted towards higher frequencies (Fig. 5). Finally, the change of the peak intensities with dot/matrix coupling reflects the frequency dependence of the Raman scattering efficiency given by Eq. (28).

### F. Size effects

In Fig. 7 is presented the size dependence of the Raman spectra of a Ge QD embedded in $SiO_2$. The calculations were performed for resonant excitation ($\delta'=0$) and the RBED is either uniform ($\Gamma'=10$) or corresponds to that of the first confined electronic transition ($\Gamma'=0.1$). The blueshift of the Raman peaks with decreasing QD size is due to both electronic- and acoustic-phonon confinement. We found that the peak frequencies are almost inversely proportional to the dot radius in agreement with the experimental findings.[25] Moreover, in Fig. 7 one can see the influence of the electronic confinement by comparing the peak frequencies, line shapes, and relative intensities for $\Gamma'=0.1$ and $\Gamma'=10$. In particular, the peak frequencies depend on the excited electronic density. For instance, for $a=2$ nm the first maximum is located around 38 cm$^{-1}$ for $\Gamma'=0.1$ and 34 cm for $\Gamma'=10$, respectively. Therefore, the analysis of peak frequencies in terms of acoustic confinement only could lead to deviations of the QD size estimated from the low-frequency Raman spectra. Moreover, let apart the resonance term (12), we found that the overall scattering efficiency increases with decreasing QD size. This is due to the fact that the electronic localization increases the contribution of high-frequency vibration modes for which the density of states is large. In addition, the coupling strength between the excited electronic states and the acoustic vibrations increases with decreasing QD size. This is shown in the inset of Fig. 7, where is plotted the squared modulus of the form factor $M_{0,0}[q(\omega)a]$ [see Eq. (28)], versus QD size. However, the dependence of the resonance factor (12) on $a$ (for a fixed $\Gamma$) increases the scattering efficiency as $a^6$. This was checked by close inspection of numerical results.

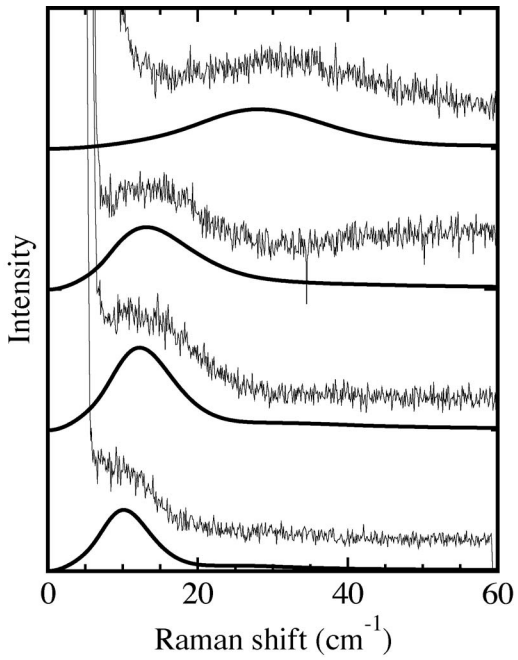


FIG. 8. Simulated and measured Stokes Raman spectra of Ge QDs embedded in $SiO_2$. The QDs average radius is $a=2.1, 3.5, 4.5$, and 5.5 nm from top to bottom. The respective standard deviations are 0.4, 1.1, 1.0, and 1.2 nm. The calculated spectra were generated using $\Gamma'=10$ (quasiuniform RBED) and assuming resonant excitation $\delta'=0$.

### III. COMPARISON WITH EXPERIMENTS

Ge nanocrystals were grown by implantation of $Ge^+$ ions in 500-nm-thick $SiO_2$, thermally grown on a (001) oriented Si wafer. Thermal annealing under nitrogen at different temperatures and for various durations[56] has been achieved. QD size distribution was measured by transmission electron microscopy with a JEOL 200CX microscope operating at 200 kV. The QDs have a spherical shape. Four samples with average radii 2.1, 3.5, 4.5, and 5.5 nm have been selected for the Raman measurements.

Raman measurements were performed at room temperature in near back-scattering geometry using a Coderg T800 spectrometer equipped with a low noise photomultiplier. The laser spot on the sample was roughly 100 $\mu m^2$ in diameter and the power was limited to about 50 mW. The excitation was the 488 nm radiation of an $Ar^+$ laser. This excitation energy (2.54 eV) was chosen to be as resonant as possible with the $E_1$-$E_1+\Delta_1$ direct electronic transitions of the Ge QDs. According to Teo *et al.*[57] the resonance is slightly higher than in bulk Ge (2.1–2.3 eV). We checked that point using different wavelengths.

The measured Raman spectra are presented in Fig. 8. They are compared to those calculated using Eq. (28) with the parameters $\Gamma'=10$ (quasiuniform RBED) and $\delta'=0$ (resonant excitation). The QDs size distributions, extracted from electron microscopy measurements have log-normal shapes, and were used as inputs in the calculations of the Raman spectra. In that way, inhomogeneous broadening of the optical transitions of the RBED and of the acoustic resonances are taken into account. The agreement between experimental and calculated spectra is satisfactory given the fact that no fitting parameters were used. In particular, the blueshift and broadening of the Raman band, with decreasing QDs average size, are rather well reproduced. As mentioned above, both homogeneous and inhomogeneous broadenings are responsible for the Raman linewidth. The detailed analysis of the Raman scattering presented in this work allows us to estimate their relative contributions. For instance, it is generally admitted that larger Raman linewidths is due to larger size dispersions. The comparison between calculated and measured spectra in Fig. 8 shows that this is not the case: the width of the Raman band increases with decreasing QDs average size, though this corresponds to similar size dispersions (19% for a radius of 2.1 nm versus 22% for a radius of 5.5 nm). One cannot, however, conclude that the homogeneous broadening increases with decreasing QD size since the acoustic mismatch is material, and not size, dependent. In fact, it is the size and frequency dependence of the excited Raman-Brillouin electronic density [i.e., form factor in Eq. (28)] that increases the Raman linewidth for the smallest QDs (see Fig. 8).

Some discrepancies between calculated and measured Raman spectra can be raised. In particular, for the smallest QDs (2.1 nm average radius), the frequency of the calculated Raman band is smaller (by 5 $cm^{-1}$), than the observed one (Fig. 8). This could be due to the rather simple description of the QD electronic structure and of the acoustic-phonon model. As a matter of fact, using a microscopic lattice dynamical model, Cheng *et al.*[58] calculated the vibration eigenmodes of Ge QDs with a diameter up to 6.8 nm. They showed that Lamb's model starts to breakdown for quantum dots with a diameter smaller than 4 nm which is consistent with our observations.

### IV. CONCLUSION

We have studied the resonant Raman scattering by acoustic vibrations in nanosized Ge QDs. The work was focused on the description of the light scattering process in the case where a large number of electronic states are involved as intermediate states. By combining them according to their contribution to the Raman efficiency, we constructed an effective electronic density which allows one to correlate the Raman spectra features to the QD's electronic structure directly. The contributions of pure and real dephasing channels to the Raman scattering were studied as a function of the QD size and homogeneous broadening of the electronic transitions. The presented approach is not specific to the Ge QDs. It can be generalized to every system where electronic localization (confinement in quantum wires and wells, in metal particles, disordered systems, etc.) determines the electron-phonon and electron-photon coupling strengths.

Matrix effects on the QD vibrations were treated in the frame of the elasticity theory. We have studied the influence of the QD/matrix acoustic mismatch on the electron-phonon interaction and on the spectral shape of the Raman

lines. The contributions of homogeneous and inhomogeneous broadenings to the Raman linewidths were estimated. Only the scattering by pure radial vibrations was considered. The calculations can be extended to include the contribution of quadrupolar vibrations, which is one order of magnitude lower, according to our evaluation for the deformation potential considered here.

The size of the QDs defines the limitations of the presented calculations. In particular, a QD with a diameter of the order of few nm cannot be assimilated to a continuous and isotropic elastic sphere. Microscopic models for the lattice vibrations and electronic states are required.

## ACKNOWLEDGMENTS

Part of this work has been supported by the French National initiative for Nanoscience (ACI.2004 nanoacoustique.NR163). A.W. acknowledges support from the EU Marie Curie Program under Contract No. HPMF-CT-2001-01281.

## APPENDIX

### 1. Averaged sound velocities

The dispersion of acoustic phonons of Ge is anisotropic. Using a comparison with molecular dynamics simulations, Saviot *et al.* [19] showed that sound velocities averaged over high symmetry directions can be used to calculate the vibration eigenmodes of a spherical QD in the frame of elasticity theory. For the mass density and elastic constants of Ge we use $\varrho_1=5.323$ and $C_{11}=1.286$, $C_{12}=0.4825$, $C_{44}=0.6680$ taken from Ref. 59. The longitudinal and transverse sound velocities averaged over the $\langle 100\rangle$, $\langle 110\rangle$, and $\langle 111\rangle$ directions, weighted by their degeneracy, are $c_l=5340$ m s$^{-1}$ and $c_t=3220$ m s$^{-1}$. In order to check the validity of this procedure, we conduct a direct averaging of the sound velocities obtained by diagonalizing the elastic dynamical matrix, weighted by the longitudinal $w_l$ or transverse $w_t$ character of the corresponding eigenmode, for random wave vector directions. We choose $w_l$ (respectively, $w_t$) to be the square of the cosine (respectively, sine) of the angle between the eigenvector and the wave vector. Several sets of 10 000 directions gave $c_l=5250\pm 7$ m s$^{-1}$ and $c_t=3288\pm 5$ m s$^{-1}$. These values were used throughout the present work. The parameters for the silica matrix are[60] $\varrho_2=2.2$, $c_{l2}=5953$ m s$^{-1}$, and $c_{t2}=3743$ m s$^{-1}$.

### 2. Acoustic eigenmodes derivation

We adapted the derivation reported in Ref. 61, for polar optical phonons, to the simpler case of acoustical phonons. The starting point is the classical theory of elasticity. For time harmonic phonon modes of pulsation $\omega$, the atomic displacements $\vec{u}$ satisfy the local equation

$$\vec{u}=-\frac{1}{q^2}\vec{\nabla}\Lambda+\frac{1}{Q^2}\vec{\nabla}\times\vec{\Gamma}, \tag{A1}$$

where $q=\omega/c_l$ and $Q=\omega/c_t$, $c_l$ and $c_t$ being the longitudinal and transverse sound velocities of the material at the point $\vec{r}$. $\Lambda=\vec{\nabla}\cdot\vec{u}$ and $\vec{\Gamma}=\vec{\nabla}\times\vec{u}$ are the divergence and curl of the displacements field, respectively. By taking the divergence and curl of Eq. (A1), $\Lambda$ and $\vec{\Gamma}$ follow the Helmholtz equations

$$\Delta\Lambda+q^2\Lambda=0, \tag{A2a}$$

$$\Delta\vec{\Gamma}+Q^2\vec{\Gamma}=\vec{0}. \tag{A2b}$$

In spherical coordinates, a general solution for the scalar Helmholtz's Eq. (A2a)

$$\Lambda=A_{l,m}z_l(qr)Y_l^m(\theta,\phi), \tag{A3}$$

where $A_{l,m}$ is an arbitrary constant and $z_l$ a spherical Bessel function. Because it simplifies the numerous recurrence relations, the spherical harmonics used for the phonons are *not normalized*.

$$Y_l^m(\theta,\phi)=P_l^m(\cos\theta)\exp(im\varphi). \tag{A4}$$

The solution of Eq. (A2b) may be written $\vec{\Gamma}=\vec{M}+\vec{N}$ with

$$\vec{M}=\vec{\nabla}\times(v_1\vec{r}), \tag{A5a}$$

$$\vec{N}=\frac{1}{Q}\vec{\nabla}\times[\vec{\nabla}\times(v_2\vec{r})], \tag{A5b}$$

$$\Delta v_i+Q^2v_i=0, \tag{A5c}$$

so that, $B_{l,m}$ and $D_{l,m}$ being arbitrary constants,

$$v_1=B_{l,m}z_l(Qr)Y_l^m(\theta,\varphi), \tag{A6a}$$

$$v_2=D_{l,m}z_l(Qr)Y_l^m(\theta,\varphi). \tag{A6b}$$

Using the curvilinear coordinates

$$\left(\vec{e}_r,\frac{\vec{X}_{lm}}{\|\vec{X}_{lm}\|},\frac{\vec{e}_r\times\vec{X}_{lm}}{\|\vec{X}_{lm}\|}\right)$$

where $\vec{X}_{lm}=\vec{L}Y_l^m/\hbar\sqrt{l(l+1)}$ is null for $l=0$ and otherwise,

$$\vec{X}_{lm}=\frac{1}{\sin\theta\sqrt{l(l+1)}}\left\{\frac{l(l-m+1)Y_{l+1}^m-(l+1)(l+m)Y_{l-1}^m}{2l+1}\vec{e}_\varphi-mY_l^m\vec{e}_\theta\right\}. \tag{A7}$$

$B_{l,m}$ drives the magnitude of $\vec{\Gamma}$ along $\vec{X}_{lm}$ and $D_{l,m}$ along the two other directions:

$$\vec{\Gamma}=D_{l,m}l(l+1)\left[\frac{z_l}{x}\right](Qr)Y_l^m\vec{e}_r-iB_{l,m}\sqrt{l(l+1)}z_l(Qr)\vec{X}_{lm}-iD_{l,m}\sqrt{l(l+1)}\left[\frac{1}{x}\frac{d}{dx}xz_l\right](Qr)\vec{e}_r\times\vec{X}_{lm}. \tag{A8}$$

Then, using Eq. (A1), a general expression for the displacements, which depend on the three variables $A$, $B$, and $D$ is found.

$$\vec{u}_{lm} = \left\{ -\frac{A_{l,m}}{q}\left[\frac{d}{dx}z_l\right](qr) + \frac{B_{l,m}}{Q}l(l+1)\left[\frac{z_l}{x}\right](Qr)\right\} Y_l^m \vec{e}_r - i\frac{D_{l,m}}{Q}\sqrt{l(l+1)}z_l(Qr)\vec{X}_{lm}$$

$$+\left\{ i\frac{A_{l,m}}{q}\sqrt{l(l+1)}\left[\frac{z_l}{x}\right](qr) - i\frac{B_{l,m}}{Q}\sqrt{l(l+1)}\left[\frac{1}{x}\frac{d}{dx}xz_l\right](Qr)\right\}\vec{e}_r \times \vec{X}_{lm}. \quad \text{(A9)}$$

*Present address: GES—UMR 5650 Université Montpellier 2/CNRS; Electronic address: jean-roch.huntzinger@univ-montp2.fr


[1] D. Kop'ev, D. Mirlin, V. Sapega, and A. Sirenko, JETP Lett. **51**, 708 (1990).
[2] V. Sapega, V. Belitsky, A. J. Shields, T. Ruf, M. Cardona, and K. Ploog, Solid State Commun. **84**, 1039 (1992).
[3] J. R. Huntzinger, J. Groenen, M. Cazayous, A. Mlayah, N. Bertru, C. Paranthoen, O. Dehaese, H. Carrère, E. Bedel, and G. Armelles, Phys. Rev. B **61**, R10547 (2000).
[4] M. Cazayous, J. R. Huntzinger, J. Groenen, A. Mlayah, S. Christiansen, H. P. Strunk, O. G. Schmidt, and K. Eberl, Phys. Rev. B **62**, 7243 (2000).
[5] M. Cazayous, J. Groenen, J. R. Huntzinger, A. Mlayah, and O. G. Schmidt, Phys. Rev. B **64**, 033306 (2001).
[6] M. Cazayous, J. Groenen, A. Zwick, A. Mlayah, R. Carles, J. L. Bischoff, and D. Dentel, Phys. Rev. B **66**, 195320 (2002).
[7] A. G. Milekhin, A. I. Nikiforov, O. P. Pchelyakov, S. Schulze, and D. R. T. Zahn, JETP Lett. **73**, 461 (2001).
[8] A. G. Milekhin, A. I. Nikiforov, O. P. Pchelyakov, S. Schulze, and D. R. T. Zahn, Nanotechnology **13**, 55 (2002).
[9] A. G. Milekhin, A. I. Nikiforov, O. P. Pchelyakov, S. Schulze, and D. R. T. Zahn, Physica E (Amsterdam) **13**, 582 (2002).
[10] H. Kushibe, M. Nakayama, and M. Yokota, Phys. Rev. B **47**, 9566 (1993).
[11] D. A. Weitz, T. J. Gramila, A. Z. Genack, and J. I. Gersten, Phys. Rev. Lett. **45**, 355 (1980).
[12] J. I. Gersten, D. A. Weitz, T. J. Gramila, and A. Z. Genack, Phys. Rev. B **22**, 4562 (1980).
[13] E. Duval, A. Boukenter, and B. Champagnon, Phys. Rev. Lett. **56**, 2052 (1986).
[14] A. Tanaka, S. Onari, and T. Arai, Phys. Rev. B **47**, 1237 (1993).
[15] A. Othmani, C. Bovier, J. C. Plenet, J. Dumas, B. Champagnon, and C. Mai, Mater. Sci. Eng., A **168**, 263 (1993).
[16] L. Saviot, B. Champagnon, E. Duval, and A. I. Ekimov, Phys. Rev. B **57**, 341 (1998).
[17] M. Fujii, Y. Kanzawa, S. Hayashi, and K. Yamamoto, Phys. Rev. B **54**, R8373 (1996).
[18] M. Pauthe, E. Berstein, J. Dumas, L. Saviot, A. Pradel, and M. Ribes, J. Mater. Chem. **9**, 187 (1999).
[19] L. Saviot, D. B. Murray, and M. C. Marco de Lucas, Phys. Rev. B **69**, 113402 (2004).
[20] N. N. Ovsyuk, E. B. Orokhov, V. V. Grishchenko, and A. Shabanin, JETP Lett. **47**, 298 (1988).
[21] Y. M. Yang, X. L. Wu, L. W. Yang, G. S. Huang, G. G. Siu, and P. K. Chu, J. Appl. Phys. **98**, 064303 (2005).
[22] P. K. Giri, R. Kesavamoorthy, B. K. Panigrahi, and K. G. M. Nair, Solid State Commun. **136**, 36 (2005).
[23] M. Fujii, T. Nagareda, S. Hayashi, and K. Yamamoto, Phys. Rev. B **44**, 6243 (1991).
[24] G. Mariotto, M. Montagna, G. Viliani, E. Duval, S. Lefranc, E. Rzepka, and C. Mai, Europhys. Lett. **6**, 239 (1988).
[25] B. Palpant, H. Portales, L. Saviot, J. Lerme, B. Prevel, M. Pellarin, E. Duval, A. Perez, and M. Broyer, Phys. Rev. B **60**, 17107 (1999), see also B. Palpant, Ph.D. thesis, Claude Bernard University, 1998.
[26] E. Duval, H. Portales, L. Saviot, M. Fujii, K. Sumitomo, and S. Hayashi, Phys. Rev. B **63**, 075405 (2001).
[27] H. Portales, L. Saviot, E. Duval, M. Fujii, S. Hayashi, N. Del Fatti, and F. Vallee, J. Chem. Phys. **115**, 3444 (2001).
[28] A. Courty, I. Lisiecki, and M. P. Pileni, J. Chem. Phys. **116**, 8074 (2002).
[29] L. Saviot and D. B. Murray, Phys. Rev. Lett. **93**, 055506 (2004).
[30] H. Lamb, Proc. London Math. Soc. **13**, 187 (1882).
[31] A. E. H. Love, *A Treatrise on the Mathematical Theory of Elasticity* (Dover, New York, 1944).
[32] E. Duval, Phys. Rev. B **46**, 5795 (1992).
[33] V. A. Dubrovski and V. Morochnik, Izv., Acad. Sci., USSR, Phys. Solid Earth **17**, 494 (1981).
[34] A. Tamura, K. Higeta, and T. Ichinokawa, J. Phys. C **15**, 4975 (1982).
[35] P. Verma, W. Cordts, G. Irmer, and J. Monecke, Phys. Rev. B **60**, 5778 (1999).
[36] M. Montagna and R. Dusi, Phys. Rev. B **52**, 10080 (1995).
[37] D. B. Murray and L. Saviot, Phys. Rev. B **69**, 094305 (2004).
[38] H. Portales, L. Saviot, E. Duval, M. Gaudry, E. Cottancin, M. Pellarin, J. Lerme, and M. Broyer, Phys. Rev. B **65**, 165422 (2002).
[39] A. A. Sirenko, V. I. Belitsky, T. Ruf, M. Cardona, A. I. Ekimov, and C. Trallero-Giner, Phys. Rev. B **58**, 2077 (1998).
[40] S. V. Gupalov and I. A. Merkulov, Phys. Solid State **41**, 1349 (1999).
[41] P. Y. Yu and M. Cardona, *Fundamentals of Semiconductors: Physics And Materials Properties*, 3rd ed. (Springer, New York, 2005).
[42] G. E. Pikus and G. L. Bir, Sov. Phys. Solid State **1**, 1502 (1960).
[43] M. P. Chamberlain, C. Trallero-Giner, and M. Cardona, Phys. Rev. B **51**, 1680 (1995).
[44] M. Cardona and F. H. Pollak, Phys. Rev. **142**, 530 (1966).
[45] F. H. Pollak and M. Cardona, Phys. Rev. **172**, 816 (1968).
[46] T. Ruf, V. I. Belitsky, J. Spitzer, V. F. Sapega, M. Cardona, and K. Ploog, Phys. Rev. Lett. **71**, 3035 (1993).
[47] T. Ruf, J. Spitzer, V. F. Sapega, V. I. Belitsky, M. Cardona, and K. Ploog, Phys. Rev. B **50**, 1792 (1994).

[48] T. Ruf, *Phonon Raman scattering in Semiconductors Quantum wells and Superlattices* (Springer, Berlin, 1998).
[49] T. Takagahara, Phys. Rev. B **60**, 2638 (1999).
[50] R. Zimmermann, Phys. Status Solidi B **173**, 129 (1992).
[51] R. Zimmermann and E. Runge, Nuovo Cimento D **D17**, 1801 (1995).
[52] R. Zimmermann and E. Runge, in *Proceedings of the 26th ICPS, Edinburgh, Scotland* (Institute of Physics, Bristol, 2002).
[53] V. I. Belitsky, A. Cantarero, S. T. Pavlov, M. Gurioli, F. Bogani, A. Vinattieri, and M. Colocci, Phys. Rev. B **52**, 16665 (1995).
[54] S. Haacke, Rep. Prog. Phys. **64**, 737 (2001).
[55] G. Bastard, *Wave Mechanics Applied to Semiconductor Heterostructures*, 1st ed. (John Wiley and Sons, Indianapolis, 1991).
[56] A. Wellner, V. Paillard, C. Bonafos, H. Coffin, A. Claverie, B. Schmidt, and K. H. Heinig, J. Appl. Phys. **94**, 5639 (2003).
[57] K. L. Teo, S. H. Kwok, P. Y. Yu, and S. Guha, Phys. Rev. B **62**, 1584 (2000).
[58] W. Cheng, S.-F. Ren, and P. Y. Yu, Phys. Rev. B **68**, 193309 (2003).
[59] J. C. Crowhurst and J. M. Zaug, Phys. Rev. B **69**, 052301 (2004).
[60] A. Polian, D. Vo-Thanh, and P. Richet, Europhys. Lett. **57**, 375 (2002).
[61] E. Roca, C. Trallero-Giner, and M. Cardona, Phys. Rev. B **49**, 13704 (1994).